

Chaotic thermohaline convection in low-porosity hydrothermal systems

Stan Schoofs^{a,*}, Frank J. Spera^b, Ulrich Hansen^c

^a *Vening Meinesz School of Geodynamics, Earth Science Institute, Utrecht University, Budapestlaan 4, 3584 CD Utrecht, The Netherlands*

^b *Department of Geological Sciences and Institute for Crustal Studies, University of California, Santa Barbara, CA 93106, USA*

^c *Institut für Geophysik, Westfälische Wilhelms-Universität Münster, Correnstraße 24, D-48149 Münster, Germany*

Received 17 February 1999; accepted 13 October 1999

Abstract

Fluids circulate through the Earth's crust perhaps down to depths as great as 5–15 km, based on oxygen isotope systematics of exhumed metamorphic terrains, geothermal fields, mesozonal batholithic rocks and analysis of obducted ophiolites. Hydrothermal flows are driven by both thermal and chemical buoyancy; the former in response to the geothermal gradient and the latter due to differences in salinity that appear to be ubiquitous. Topographically driven flows generally become less important with increasing depth. Unlike heat, solute cannot diffuse through solid matrix. As a result, temperature perturbations advect more slowly than salinity fluctuations by the factor ϕ , but diffuse more rapidly by the factor κD and are so smoothed out more efficiently. Here, ϕ is porosity, while κ and D denote the thermal and chemical molecular diffusivity, respectively. Double-advective instabilities may play a significant role in solute and heat transport in the deep crust where porosities are low. We have studied the stability and dynamics of the flow as a function of ϕ and thermal and chemical buoyancy, for situations where mechanical dispersion of solute dominates over molecular diffusion in the fluid. In the numerical experiments, a porous medium is heated from below while solute provides a stabilizing influence. For typical geological parameters, the thermohaline flow appears intrinsically chaotic. We attribute the chaotic dynamical behavior of the flow to a dominance of advective and dispersive chemical transfer over the more moderate convective heat transfer, the latter actually driving the flow. Fast upward advective transport and lateral mixing of solute leads to formation of horizontal chemical barriers at depth. These gravitationally stable interfaces divide the domain in several layers of distinct composition and lead to significantly reduced heat flow for thousands of years. The unsteady behavior of thermochemical flow in low-porosity regions has implications for heat transport at mid-ocean ridges, for ore genesis, for metasomatism and metamorphic petrology, and the diagenetic history of sediments in subsiding basins. © 1999 Elsevier Science B.V. All rights reserved.

Keywords: thermohaline circulation; convection; porous materials; geothermal systems; chaos; numerical model

1. Introduction

Virtually all of the oceanic crust to depths of 5–7 km, and also continental crust at depths greater

* Corresponding author. Tel.: +31-30-253-5142;
Fax: +31-30-253-5030; E-mail: schoofs@geo.uu.nl

than several kilometers, is characterized by a porosity which is as small as one volume percent or less [1–3]. Aqueous fluids are present down to at least 9 km, based on deep borehole measurements [4–6] and analysis of obducted ophiolites, e.g. [7]. Further, it has been argued from oxygen isotope systematics of exhumed metamorphic terrains that fluids may penetrate down to 10–15 km [8]. The extensive collected works of Taylor and co-workers (see [9] for a compilation) and others readily demonstrates the pervasive role played by fluids in mediating transport of heat and chemicals with the Earth's crust.

Large volumes of the Earth's crust although of low porosity may be fluid-saturated. Provided sufficient permeability exists, these fluids advect within the deeper crust, driven by both thermal and chemical buoyancy; the former in response to the geothermal gradient and the latter due to local variations in salinity, an almost inevitable consequence of complex geologic processes. For example, very general and global mechanisms produce gradients in the salt concentrations within the fluid: meteoric water recharge from above (e.g. rain) while diagenetic, metamorphic and/or magmatic fluid sources lead to high concentrations of dissolved elements (up to saturation level) deeper within the crust, e.g. [10]. Advection of the saline fluids through the rocks has implications for many geological processes, such as heat transport, ore genesis, metasomatism and metamorphic petrology, and including the diagenetic history of sediments in subsiding basins [11–16]. For an overview of these and other hydrogeological implications, the reader is referred to Person et al. [17] and Ingebritsen and Sanford [18].

When a fluid moves through a porous medium, heat and chemical elements can be transported by (1) diffusion through the interstitial liquid, (2) advection of the liquid and (3) molecular diffusion through the solid matrix. While diffusion of heat through the solid and liquid is of the same order, diffusion of chemical components through the liquid is much larger than through the solid. In addition to advective and diffusive transport of chemical elements, hydrodynamic mixing of the interstitial fluid at the pore scale also leads to chemical transfer. This type of mixing, also called

mechanical dispersion, is due to obstructions and the fact that all pores may not be accessible to a fluid element after it has entered a particular flow path [19]. Due to substantial heat diffusion through the solid rocks, mechanical dispersion of heat in the liquid is negligible under most geological circumstances [20,21].

Heat and dissolved elements thus influence the interstitial fluid density in a different manner. Heat advects slower than chemical elements through the liquid by the factor ϕ , while diffusion of heat through the bulk porous medium is larger by the factor ϕ^{-1} times the ratio between the thermal and chemical diffusivities [22]. Since the porosities are quite low of the order 10^{-2} – 10^{-4} in the deeper crust, double-advective double-diffusive instabilities may play a large role in the transport of solute and heat.

In this study, the stability and dynamics of the flow as a function of ϕ and thermal and chemical buoyancy are investigated, for situations where dispersion of solute dominates over molecular diffusion in the fluid. In our numerical experiments, the low-porosity medium is heated from below, while solute provides a stabilizing influence.

The outline of the paper is as follows. In Section 2, the governing equations describing thermohaline convection in a porous medium and the employed numerical method are given. The stability and dynamics of thermochemical convection in low-porosity media are described in Section 3. After demonstrating a few possible evolutionary states of the flow, we discuss the general picture of the fluid dynamical behavior as a function of the thermal and chemical buoyancy and porosity. Furthermore, the sensitivity of the convective flow to the anisotropic and dispersive character inherent to rocks is discussed. We conclude the paper by summarizing the results and discussing the geological implications of this work.

2. Formulation

We have considered a two-dimensional homogeneous porous medium in a square domain,

which is saturated with fluid (see Fig. 1). The horizontal and vertical Cartesian coordinates are denoted by x and z , respectively. In reality, thermochemical convection in porous media is evidently three-dimensional [23]. However, the essential physics involving low-porosity thermochemical convection are captured in a two-dimensional model [22]. Furthermore, modeling of low-porosity convection is numerically challenging, because the allowed time step size depends linearly on ϕ . Therefore, we feel that a study with good resolution in two dimensions fits our purposes better than a three-dimensional one on a rather coarse grid.

Conservation of mass of fluid in a porous medium is described by:

$$\nabla \cdot \mathbf{q} = 0 \quad (1)$$

where it is assumed that the fluid is incompressible [20]. This so-called Boussinesq approximation is reasonable when the fluid remains in the single-phase regime and temperature contrasts do not vary much across the domain [18]. Here, \mathbf{q} is the seepage velocity.

Assuming that inertia effects are negligible, conservation of momentum in the porous medium can be expressed by the empirical law of Darcy [24]:

$$\mathbf{q} = -\frac{\mathbf{K}}{\mu} (\nabla p - \rho \mathbf{g}) \quad (2)$$

with p for pressure, ρ for fluid density and \mathbf{g} for the gravitation vector. The permeability \mathbf{K} vector, consisting of the horizontal permeability K_x and the vertical component K_z , is assumed to be spatially invariant and isotropic in most experiments. However, a few experiments in strongly anisotropic media have also been performed. The orientation of the principal axes of \mathbf{K} are assumed to be parallel to the sides of the domain. For the situation of an arbitrary orientation of coordinate axes, the reader is referred to Tyvand and Storeletten [25]. The dynamic fluid viscosity μ is taken as a constant.

It is assumed that the fluid and matrix are in thermal equilibrium; conservation of energy can

then be expressed as:

$$\sigma \frac{\partial T}{\partial t} - \kappa \nabla^2 T + \mathbf{q} \cdot \nabla T = 0 \quad (3)$$

where T denotes the temperature and κ , the effective thermal diffusivity of the saturated medium, is constant. Further, σ represents the ratio of the heat capacities between the solid matrix and the fluid $\sigma = \phi + (1 - \phi)(\rho c_p)_{\text{matrix}} / (\rho c_p)_{\text{fluid}}$. Here, c_p represents the isobaric heat capacity and ϕ is the porosity of the medium.

When we assume that the dispersive flux of chemical concentration can be expressed in Fickian form, conservation of the solute concentration C is given by [26]:

$$\phi \frac{\partial C}{\partial t} - \nabla \cdot (\mathbf{D}_h \nabla C) + \mathbf{q} \cdot \nabla C = 0 \quad (4)$$

where \mathbf{D}_h is a second-order tensor which describes the hydrodynamic dispersion [19]. The tensor consists of the summation of the molecular diffusion in the porous medium, \mathbf{D}_{mol} , and the tensor of mechanical dispersion \mathbf{D}_{mech} . Here, the molecular diffusion in the porous medium is defined as $\mathbf{D}_{\text{mol}} = \phi \mathbf{D}_w / \tau$, where \mathbf{D}_w is the molecular diffusivity of the chemical component within the fluid and τ the tortuosity of the porous medium. The coefficients of \mathbf{D}_{mech} are:

$$(\mathbf{D}_{\text{mech}})_{ij} = (a_l - a_t) \frac{q_i q_j}{|\mathbf{q}|} + a_t |\mathbf{q}| \delta_{ij} \quad (5)$$

where a_l and a_t represent the longitudinal and transversal dispersivities, respectively, and δ_{ij} is the Kronecker delta. In general, mechanical dispersion of chemical concentration is more important than molecular diffusion, except when the flow is very slow.

The laws for conservation of mass, momentum, energy, species and a linearized equation of state $\rho = \rho_0 [1 - \alpha(T - T_0) + \beta(C - C_0)]$ (reference values are denoted by the subscript 0) describe thermochemical convection in porous media mathematically. Here, α and β are the coefficients of thermal and chemical expansion, respectively. The equations are non-dimensionalized with the height of the domain h as the length scale, $h^2 \sigma / \kappa$ as time-scale, K_v as the permeability scale, $\mu \kappa / K_v$ as dynamic pressure scale and $\Delta T = T_1 - T_0$ and

$\Delta C = C_1 - C_0$ as the temperature and chemical scale, respectively (maximum values of T and C are denoted by the subscript 1). This results in the following set of differential equations:

$$\frac{\partial \hat{p}}{\partial \hat{x}} K_r \frac{\partial \hat{p}}{\partial \hat{x}} + \frac{\partial^2 \hat{p}}{\partial \hat{z}^2} = Ra_C \frac{\partial \hat{C}}{\partial \hat{z}} - Ra_T \frac{\partial \hat{T}}{\partial \hat{z}} = \frac{\partial \hat{p}^*}{\partial \hat{z}} \quad (6)$$

$$\frac{\partial \hat{T}}{\partial \hat{t}} - \nabla \cdot (\hat{\kappa} \nabla \hat{T}) + \hat{q} \cdot \nabla \hat{T} = 0 \quad (7)$$

$$\begin{aligned} \phi^* \frac{\partial \hat{C}}{\partial \hat{t}} + \hat{q}_x \frac{\partial \hat{C}}{\partial \hat{x}} + \hat{q}_z \frac{\partial \hat{C}}{\partial \hat{z}} = \\ \frac{\partial}{\partial \hat{x}} \left(\left(f_1 + \frac{1}{Le_{mol}} \right) \frac{\partial \hat{C}}{\partial \hat{x}} + f_3 \frac{\partial \hat{C}}{\partial \hat{z}} \right) + \\ \frac{\partial}{\partial \hat{z}} \left(f_3 \frac{\partial \hat{C}}{\partial \hat{x}} + \left(f_2 + \frac{1}{Le_{mol}} \right) \frac{\partial \hat{C}}{\partial \hat{z}} \right) \end{aligned} \quad (8)$$

where:

$$f_1 = \frac{\hat{a}_t (a_r \hat{q}_x^2 + \hat{q}_z^2)}{|\hat{q}|}, \quad f_2 = \frac{\hat{a}_t (a_r \hat{q}_z^2 + \hat{q}_x^2)}{|\hat{q}|},$$

$$f_3 = \frac{\hat{a}_t ((a_r - 1) \hat{q}_x \hat{q}_z)}{|\hat{q}|}$$

Here, the circumflexes denote the non-dimensionality of a parameter. Moreover, $\hat{p}^* = \hat{p} - \hat{p}_0 = Ra_C \hat{C} - Ra_T \hat{T}$ is the difference between the density and the density at the reference state. The five dimensionless parameters governing the convective dynamics are the thermal Rayleigh number Ra_T , the chemical Rayleigh number Ra_C , the permeability ratio K_r , ϕ^* , a_r and the Lewis number, Le_{mol} . These dimensionless parameters are defined as:

$$Ra_T = \frac{\alpha K_z \rho_0 g \Delta T h}{\kappa \mu}, \quad Ra_C = \frac{\beta K_z \rho_0 g \Delta C h}{\kappa \mu},$$

$$K_r = \frac{K_x}{K_z}, \quad \phi^* = \phi / \sigma, \quad a_r = a_l / a_t, \quad Le_{mol} = \frac{\tau \kappa}{D_w}$$

Besides the two Rayleigh numbers, their ratio is also used in this study. This so-called buoyancy

ratio R_p is given by:

$$R_p = \frac{Ra_C}{Ra_T} = \frac{\beta \Delta C}{\alpha \Delta T}$$

The heat capacity ratio is assumed to be equal to $\sigma = 1$ in this study, a reasonable assumption for most natural systems. That is, since $(\rho c_p)_{matrix} \approx (\rho c_p)_{fluid}$, $\sigma = 1 - \phi$ which goes to unity for ϕ small. Scale analysis of Eqs. 7 and 8 shows that non-dissolvable elements are advected at the fluid velocity \hat{q}/ϕ^* , while temperature advects with the total fluid flux \hat{q} . This leads to the development of double-advective, double-diffusive instabilities [22], especially in geological media of low porosity.

Fig. 1 displays the configuration of the model together with the boundary conditions. A square domain with impermeable boundaries is considered. The temperature and chemical concentration at the bottom boundary are equal to one, while at the top, both quantities are fixed to zero. The vertical walls are insulators with respect to heat and solute transport. Initially, the fluid is motionless and the dynamical pressure distribution is zero everywhere. The interior is cold and chemically depleted. Note that heat destabilizes the liquid, while the solute provides a stabilizing influence.

At each time step, temperature and salinity are used to compute the horizontally averaged heat and solute fluxes at the surface. The heat flow through the surface of the domain is defined as:

$$q_T = -\lambda \overline{\frac{\partial T}{\partial z}}; \quad \text{at } z = 0 \text{ m} \quad (9)$$

where λ ($= 2.5 \text{ W/m}^\circ\text{C}$) denotes the thermal conductivity and the overbar implies a horizontal average. The chemical surface flux is defined as:

$$q_C = -\overline{(D_h \nabla C)_z}; \quad \text{at } z = 0 \text{ m} \quad (10)$$

The system of Eqs. 6–8 is solved on a cell-centered grid by using a second-order finite volume multigrid method. Details of the method are given by Trompert and Hansen [27], where it was used for free convection at infinite Prandtl number.

Spatially, a central approximation is used for the diffusive fluxes. Furthermore, the flux-limited Fromm scheme [28] is used for the advective compositional fluxes to preserve the monotonicity of the solution at sharp interfaces. The non-limited version of this scheme is used for the advective thermal fluxes.

Time integration is carried out by the implicit second-order Crank–Nicolson method for the diffusion of heat. The second-order explicit Adams–Bashforth scheme is used to advance the advective terms of the energy and species equation in time. This Adams–Bashforth scheme is also employed for the velocity-dependent chemical dispersion terms. Validation of the code was accomplished by comparison with published results on thermal and thermochemical convection in porous media [29–31].

3. Results: dynamics of low-porosity thermohaline convection

In this section, the stability and dynamics of thermohaline convection in low-porosity media are investigated for the case in which the porous medium is heated from below, while chemical concentration provides a stabilizing influence. We investigate the case in which mechanical dis-

persion of the solute dominates over molecular diffusion of the solute within the fluid. First, the results of a few numerical experiments are presented to give an overview of the possible evolutionary states (Section 3.1). Next, the evolutionary states of the first set of experiments are discussed for a variety of porosities. Finally, the sensitivity of the fluid dynamical behavior to the anisotropic permeability and dispersive character of the rock is discussed (Section 3.3). The spatial numerical resolution used is 64×64 grid cells, based on extensive testing with other (also finer) discretizations and smaller time step sizes. The grid cells are refined in vertical direction near the base and the top of the domain in order to resolve the horizontal boundary layers.

3.1. Flow dynamics and transport properties: a few examples

In a first set of experiments, the thermal Rayleigh number Ra_T , the buoyancy ratio R_p and the porosity ϕ of the medium are varied systematically. All sides of the system are impermeable (see Fig. 1). Furthermore, permeability and porosity are isotropic and homogeneous throughout the domain. The transversal dispersivity is 5×10^{-5} times the vertical length scale of the domain, while the dispersivity ratio is equal to $a_r = 10$. Initially, the motionless fluid is cold and chemically depleted, while the fluid is perturbed by giving the lower left grid point a temperature $\hat{T} = 0.1$.

Within the whole set of experiments, we have observed the system evolving to one of the following states: (1) static diffusive, (2) steady convective, (3) oscillatory convective and (4) chaotic convective. The system of equations is integrated numerically until one of the stages can be clearly distinguished. At this point, (1) the average velocity is smaller than 10^{-4} and the heat flux through the domain is purely diffusive, (2) the average velocity is larger than 10^{-4} and the difference between the surface heat flow and the globally averaged heat flow is smaller than 10^{-4} , (3) at least five similar periods of the oscillation have been observed and finally, (4) a statistically steady state has been reached.

Apart from the obvious static, diffusive solu-

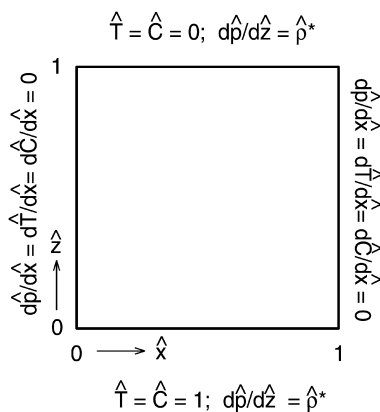


Fig. 1. Geometrical setup and boundary conditions of the experiments in a porous medium, which is heated and salted from below. Initially, both temperature \hat{T} and chemical concentration \hat{C} equal zero.

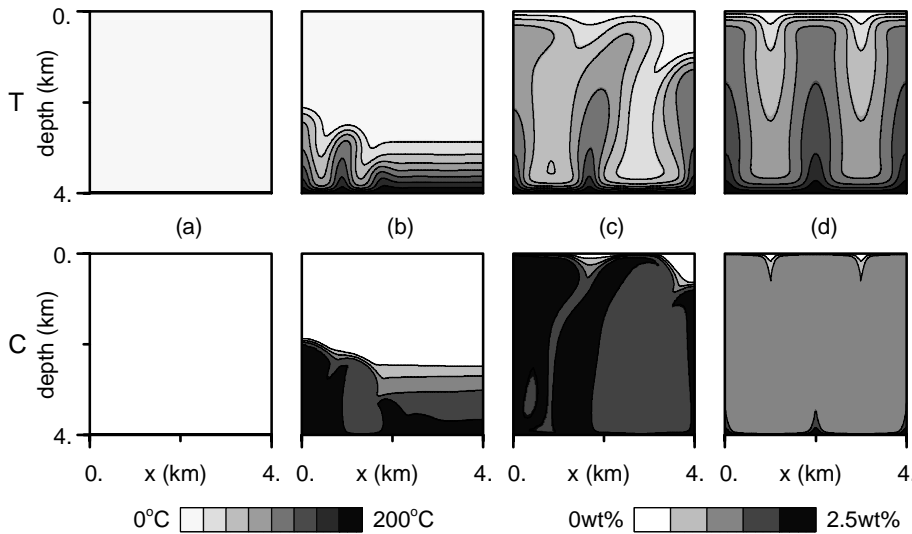


Fig. 2. Snapshots of temperature T and compositional concentration C fields of a simulation with $\Delta C=2.5$ wt% and $\phi=0.01$ at (a) $t=0.0$ kyr, (b) $t=8.0$ kyr, (c) $t=40.0$ kyr and (d) $t=200.0$ kyr. The corresponding dimensionless parameters are $Ra_T=600$, $R_p=0.25$. The contour intervals are 25°C and 0.5 wt%, respectively (see legends). Flow evolves towards steady state solution.

tion, the observed evolutionary states of the flow are elucidated in three examples with $Ra_T=600$ and a porosity of $\phi=0.01$. Dimensional parameters are used in the following, in order to give a better impression of the geological implications of the flow. The depth of the system is $H=4$ km, the temperature difference across the domain is $\Delta T=200^\circ\text{C}$ and permeability is $K=6 \times 10^{-14}$ m². Further, $\rho_0=10^3$ kg/m³, $\mu=5 \times 10^{-4}$ Pa s, $\beta=10^{-4}$ wt%⁻¹, $\alpha=10^{-3}\text{C}^{-1}$ and $\kappa=6 \times 10^{-7}$ m²/s.

In Fig. 2a–d, the temperature and chemical distributions are depicted at four stages during the evolution of an experiment with a low chemical contrast of $\Delta C=2.5$ wt% between top and bottom (corresponding with $R_p=0.25$). A dark (light) shading indicates a high (low) temperature or chemical concentration. Initially, a thermal boundary develops diffusively at the bottom of the domain, which quickly becomes unstable (Fig. 2a,b). The thermally driven convective flow entrains salinity dispersively through the bottom of the domain into the interior (Fig. 2b,c). Due to the low buoyancy of the chemicals, there is not much hindering force. The flow is therefore able to evolve rapidly towards a convective steady state, in this

case consisting of four side-by-side slender cells (Fig. 2d). The steady flow is characterized by three ascending plumes of hot fluid and two sinking colder currents in between. Note that solute advects 100 times faster than heat in this simulation. Thin thermal and even thinner chemical boundary layers are visible at the top and bottom of the domain. Since the solute transport is dominated by advection and/or dispersion throughout the domain, the interior is chemically well-mixed and nearly homogeneous at an average of $C=1.25$ wt%.

Fig. 3 shows the T and C distributions at four stages of an experiment with a slightly larger chemical contrast of $\Delta C=4$ wt% between top and bottom. During the first 10^5 years of the evolution, an irregular flow pattern is visible (Fig. 3a), consisting of several irregular convection cells. The system frequently bifurcates to a flow pattern with another number of the cells. Note that diffusive areas, indicated by gradually increasing temperature and chemical concentration with depth (for example, the right-hand side of the domain in Fig. 3a), coexist with adjacent convecting fluid. While the temperature field remains smooth, vigorous advection of the solute mixes

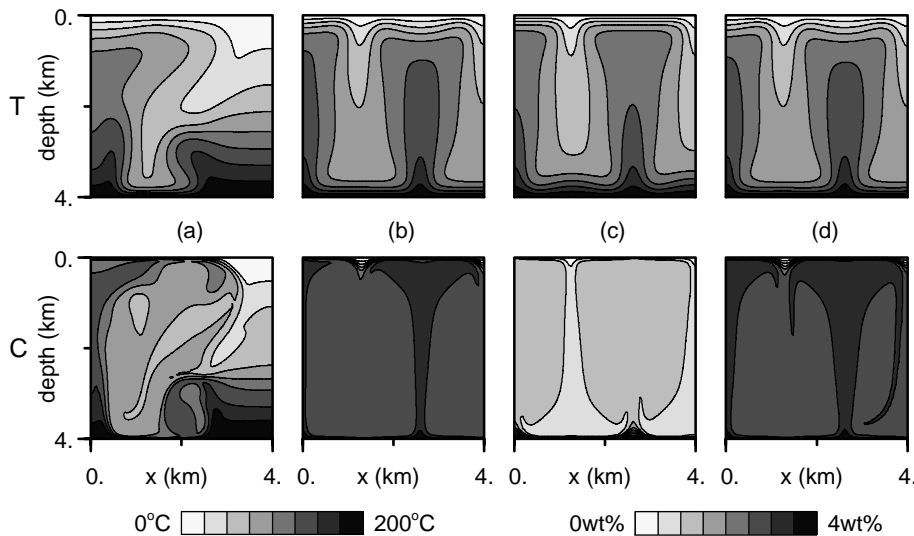


Fig. 3. Temperature and solute snapshots of a flow which evolves towards an oscillatory state. The parameters are similar to those in Fig. 2, except $\Delta C = 4$ wt% ($R_p = 0.4$). The corresponding times are (a) $t = 112.8$ kyr, (b) $t = 513.6$ kyr, (c) $t = 535.6$ kyr and (d) $t = 2736$ kyr. The contour intervals are 25°C and 0.5 wt% again.

the solute very well in these advective parts of the domain. As a result, these advective parts appear as chemically almost homogeneous spots, while sharp interfaces separate the diffusive and advective environments. Note that within the convective areas, a significant amount of fluid recirculates.

Suddenly, the convection evolves towards a spatially coherent flow pattern of three side-by-side cells (Fig. 3b). Due to the slightly unstable thermal boundary layers, variable amounts of chemical concentration enter or leave the domain dispersively through the bottom and top. As a result, the chemical content of the interior varies in an oscillatory fashion between $\Delta C = 0.5$ and 3.5 wt%, with a period of 6 kyr (see Fig. 3b–d).

Fig. 4 displays the thermal and chemical distributions for an even larger chemical difference between the horizontal sides of the domain ($\Delta C = 10$ wt%), at five different stages in the evolution. Fig. 4a shows a hybrid pattern of advective and diffusive areas. In contrast to the previous experiment, the flow remains chaotic and reaches a statistically steady state. We attribute the chaotic behavior at larger chemical contrasts to the fact that the thermochemical system is dominated by advection, in

this case, of principally one component: chemical concentration.

Another characteristic feature of the flow at low porosity is the spontaneous development of horizontal chemical barriers at depth. These gravitationally stable interfaces divide the domain into two or more separately convecting layers of a different chemical content. Rather than being an exception, the interface development is a common and prominent feature observed in low-porosity flow.

The formation and evolution of one of these interfaces is shown in Fig. 4b–e. In Fig. 4b, the interface is visible as the clustering of several horizontal isopleths at a depth of 2.4 km. Further convective mixing within the layers adjacent to the interface results in an increase of the chemical and thus density contrast across the interface up to a maximum of $\Delta C = 9$ wt% (Fig. 4c).

When the convective vigor in the lower layer increases, fluid is entrained convectively from above the interface into the lower layer. Consequently, the density interface gradually migrates upward until it merges with the upper boundary layer, such resulting in a single layered flow again (Fig. 4c–e). Note that besides upward moving in-

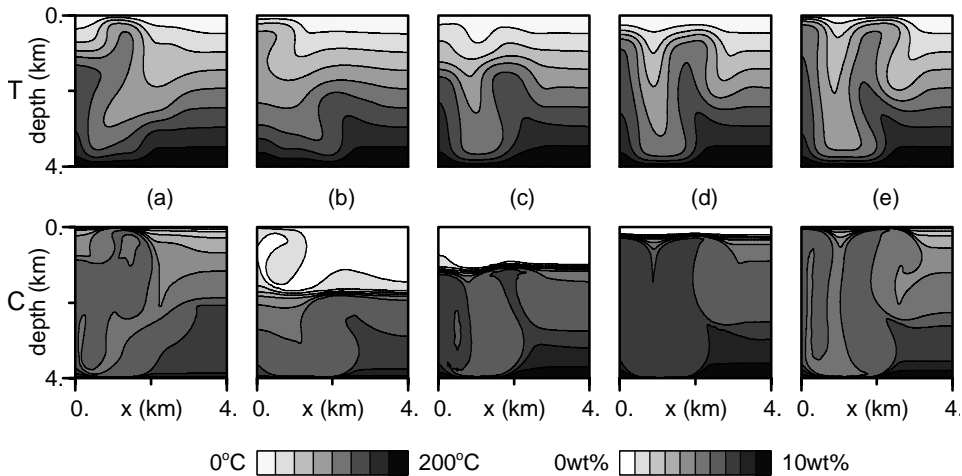


Fig. 4. Temperature and salinity snapshots of a flow which remains chaotic. Parameters are similar to those in Figs. 2 and 3, except $\Delta C = 10$ wt% ($R_p = 1.0$). Snapshots b–e describe a cycle of the generation, migration and disappearance of a chemical interface at depth. The corresponding times are (a) $t = 312.6$ kyr, (b) $t = 320.2$ kyr, (c) $t = 325.0$ kyr, (d) $t = 327.2$ kyr and (e) $t = 329.4$ kyr. The contour interval is 25°C in the temperature plots and 1 wt% in those of chemical concentration.

terfaces, we have also observed several interfaces migrating downward in the same experiment. For downward migration to occur, convection in the upper layer has to be more vigorous as compared to that in the lower layer. The migration of den-

sity interfaces which developed in an initially linearly stratified chemical concentration field is discussed in more detail by Schoofs et al. [32,33].

Besides elucidating the various possible evolutionary states of the system, the three examples

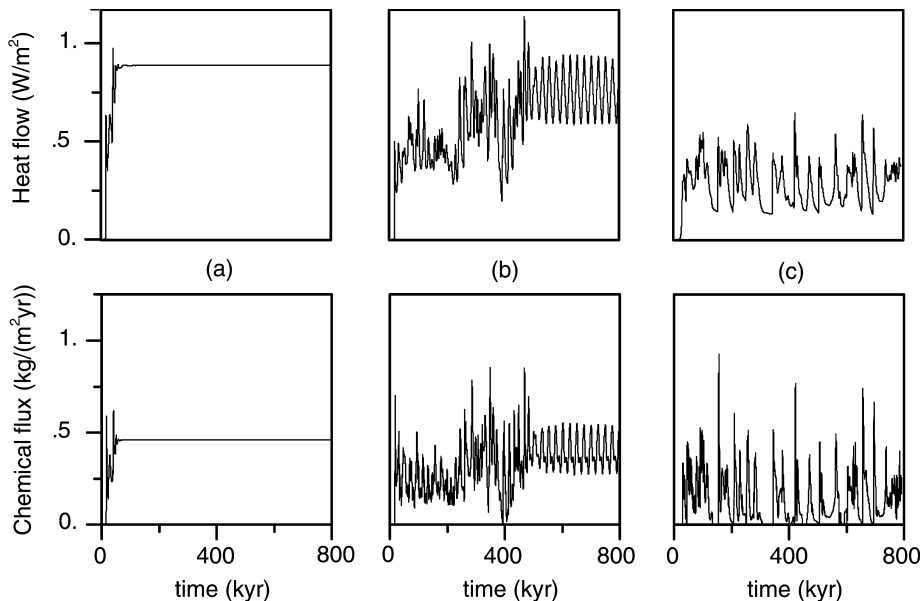


Fig. 5. (a–c) Temporal evolution of the heat and solute fluxes through the top of the domain for the experiments depicted in Figs. 2, 3 and 4, respectively.

show an important effect of the chemically dissolved elements. Despite the stabilizing influence of salinity on the density profile, increasing the salinity difference between top and bottom results in a transition from steady to chaotic behavior. At the threshold value of the chemical to thermal buoyancy ratio, the convection is often characterized by an oscillatory flow pattern. We attribute this transition to an increasing influence of the transport of chemicals over the thermally driven flow field. The flow, although driven by a moderate thermal difference, appears intrinsically unsteady due to the advectively and dispersively dominated transport of the solute.

In Fig. 5, the temporal evolution of the heat and chemical fluxes through the top of the domain are shown for the three examples. For the experiment with the lowest chemical contrast, the system evolves quickly to a steady state (Fig. 5a,d). For the intermediate chemical contrast ($\Delta C=4$ wt%), both heat and solute transport become oscillatory after an initial stage of chaotic flow behavior (Fig. 5b,e). When $\Delta C=10$ wt% (Fig. 5c,f), finally, both surface fluxes remain un-

steady up to the end of simulation. Furthermore, the time-average of the chaotic heat flux is reduced as compared to the fluxes at a lower chemical contrast, because a part of the internal energy which enters the domain through the bottom is used to transport the dense chemical elements upwards. Finally, heat (solute) fluxes are reduced especially during those periods in which an interface is present, because transport across this barrier is mainly diffusive (dispersive) [32,33].

The shortest observed periods of the chemical flux are of the order of a few decades. These fluctuations are due to the variations in the chemical content of the advected fluid which reach the top of the domain. The highest frequency fluctuations are not present in the heat flux curves, because heat diffuses faster and advects at a slower rate as compared to solute. The periods between the large amplitude fluctuations correspond with the time needed for the formation and disappearance of the chemical interfaces. These time periods are therefore related directly to the migration speed of the interfaces.

The petrological evolution of the host rock de-

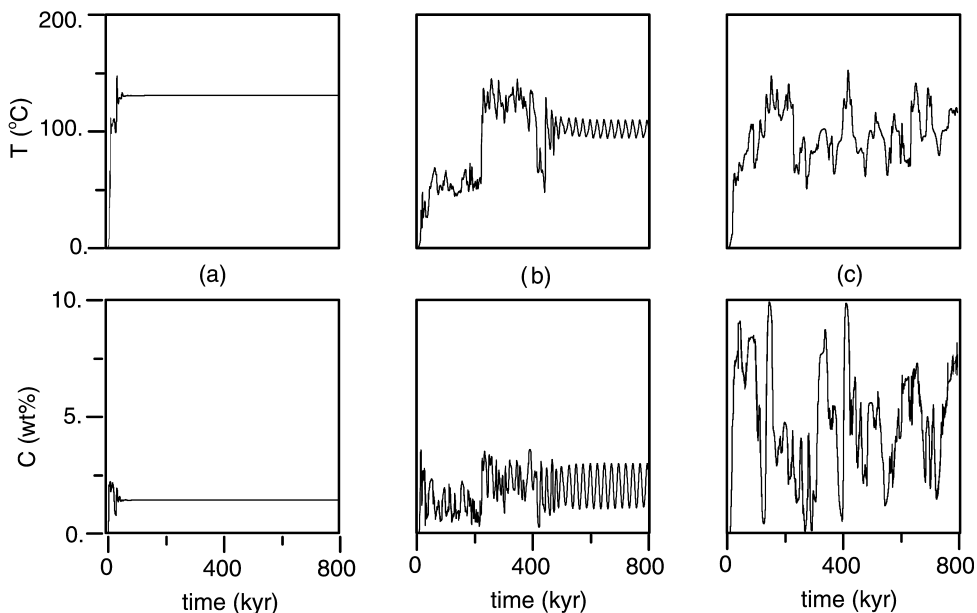


Fig. 6. Temporal evolution of temperature (upper panels) and salinity (lower panels) at the center of the domain ($x=z=2.0$ km). (a) $\Delta C=2.5$ wt%, (b) $\Delta C=4$ wt%, (c) $\Delta C=10$ wt%.

pends significantly on the temperature and salinity of the fluid at a fixed location. Therefore, we have plotted the temporal evolution of T and C at the center of the domain for the three simulations (see Fig. 6). Obviously, the dynamical behavior of the flow is reflected directly in the thermal and chemical evolution of the fluid and thus the host rock. For the chaotic case, the migration of chemical interfaces results in salinity variations of up to $\Delta C = 9$ wt% on timescales as short as a few decades. The flushing of the rocks with fluid of a highly variable solute content may lead to alternating periods of over- and undersaturation of chemicals within the fluid. Precipitation and dissolution of typical chemical elements could then easily produce the zonation, typically found in metamorphic rocks (e.g. banded sphalerite) [34].

Due to significant diffusion of heat, the thermal history of the rock is smoother as compared with the chemical one. Nevertheless, fluctuations up to half of the imposed temperature contrast between top and bottom are observed within periods of the order of 1000 years.

Results on the petrological history of a rock, as inferred from methods like oxygen isotope analysis [9] or fluid inclusion techniques [35], are therefore very sensitive to the typical convective style of the flow. Salinities of distinct populations of preserved fluid inclusions within crystalline phases from many geothermal (including ore-forming) regions are very commonly found [35,36]. The origin of these distinct populations may be related to the instabilities modeled in this study.

3.2. Flow regimes at various porosities

After discussing the possible evolutionary states of the system, we concentrate now on the distribution of these states within the Ra_T – R_p – ϕ space which was sampled by our numerical experiments. Dimensionless parameters are used in order to give a more general picture. The flow space is plotted in Fig. 7a–c for three porosities, as a function of Ra_T and R_p . The four different symbols denote the evolutionary states of the system and are explained in the figure caption.

Fig. 7a shows the first case in which the medium has an hypothetical porosity of $\phi = 1$, which

means that heat and solute advect with the same speed through the porous medium. At low buoyancy ratios, $R_p \leq 0.25$, the flow evolves to a steady or oscillatory convective solution when the thermal Rayleigh number is large enough to destabilize the fluid. Here, this critical Rayleigh number $Ra_{T,cr}$, increases gradually with increasing buoyancy ratio. For increased buoyancy ratios, chaotic flows generically evolve. Note that for pure thermally driven convection ($R_p = 0$), the transition from oscillatory to chaotic convection occurs between $Ra_T = 600$ and 1000, that is, at a higher value than for thermochemical convection.

Neither density interfaces or diffusive areas were observed in any of the experiments with $\phi = 1$, in contrast to flow at low porosity ($\phi = 0.01$). Instead, convective currents directly connect the top and bottom of the system. The unsteady behavior of the flow is due to unstable boundary layers and cell bifurcations.

Fig. 7b shows the flow space for the case when the medium has an intermediate porosity of $\phi = 0.1$. In most of the simulations, the flow evolves through a stage of irregular convective flow towards a static diffusive solution. During the chaotic stage in the evolution, the convective currents connect the top and bottom of the system again, while the formation of density interfaces is not observed. Diffusive areas do exist alongside convective patches within the flow domain, however, like in the low-porosity experiment shown in Fig. 4. Despite the uniform heating and salting of the interior through the bottom, the difference in advection velocity of heat and solute apparently concentrates the vertical transfer of these quantities in laterally bounded areas.

At low porosity of the medium ($\phi = 0.01$), finally, the convective dynamics appear chaotic in nearly all simulations (see Fig. 7c). The flow is characterized by diverse, complex flow patterns, consisting of, first, the coexistence of diffusive and convective domains and, next, the formation, migration and disappearance of horizontal density interfaces. The dynamical behavior of the flow in low-porosity media is therefore fundamentally different from flow at higher porosity. The manifestation of this instability at typically low porosity is visible in Fig. 7d, where the evolutionary states

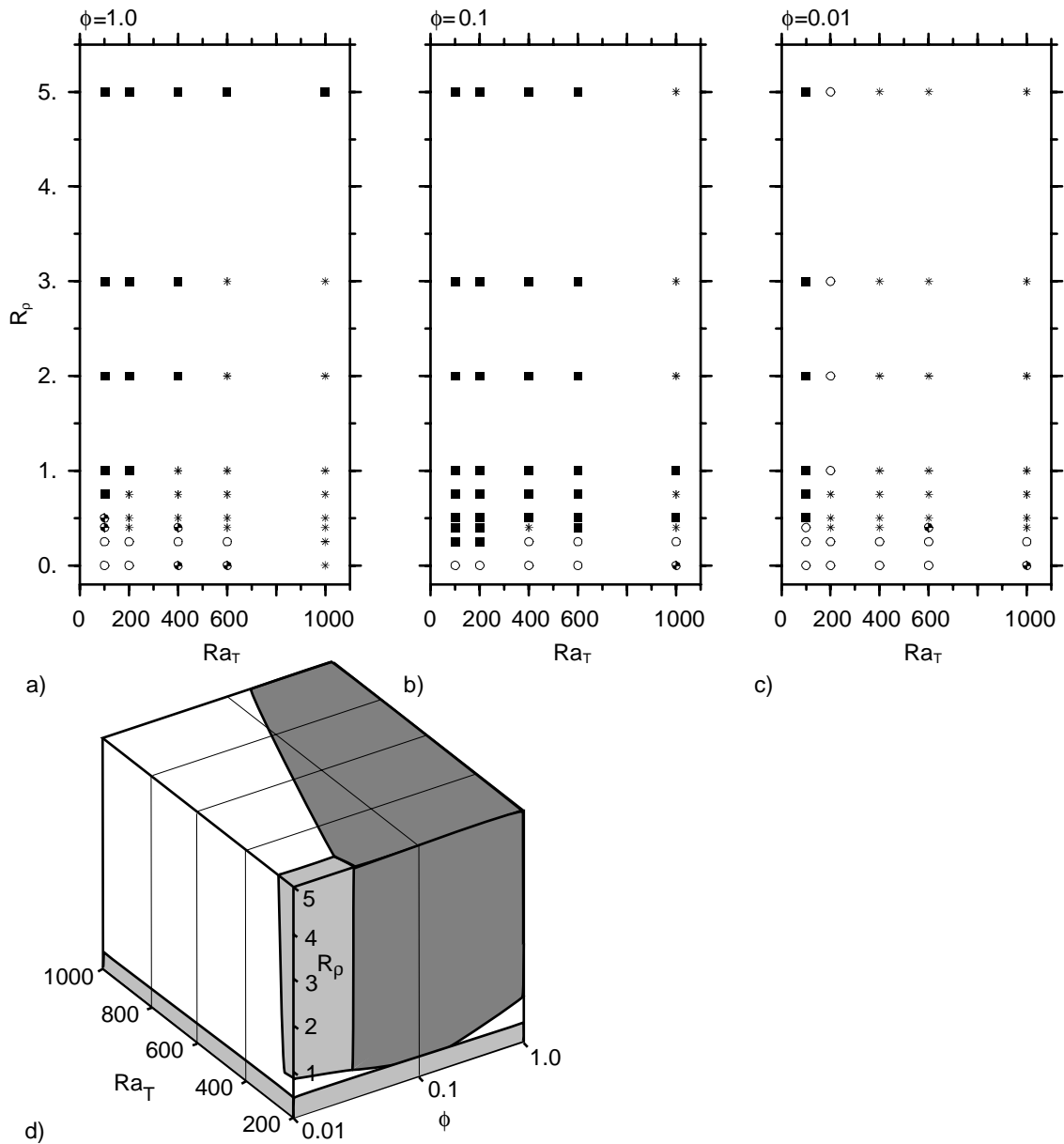


Fig. 7. Evolutionary states of the system in Ra_T – R_p space for (a) porosity equal to $\phi=1$, (b) $\phi=0.1$ and (c) $\phi=0.01$. Here, (1) a solid square indicates a static diffusive, (2) open circle a steady convective, (3) balloon an oscillatory convective and (4) an asterisk denotes a chaotic convective state. (d) Same evolutionary states, but now plotted on the surface of a cube with axes Ra_T , ϕ and R_p , as to show the appearance of the chaotic (white) regime at low porosity. The light-gray regimes include both steady and oscillatory convective states, while the flow evolves towards the static diffusive state in the dark-gray shaded regime.

are plotted on the surface of a cube with axes Ra_T , ϕ and R_p .

A few exceptions from the almost intrinsically unsteady character of the thermohaline driven

flow at low porosity are observed. Apart from the obvious static diffusive solution which is obtained when the thermal buoyancy is not large enough to even drive convection without the pres-

ence of solute, the flow evolves to a steady or oscillatory state when $R_p \leq 0.4$, similar to the flow at the higher porosities. Furthermore, in the regime of low thermal Rayleigh numbers ($Ra_T = 200$) and large buoyancy ratios, a steady state solution is obtained consisting of a few side-by-side slender cells. The chemical horizontal boundary layers are completely embedded in the thermal ones, due to low chemical dispersion as compared to thermal diffusion. Since the chemical field ‘freezes’ at the moment that the flow reaches the steady state, the ultimate spatial averaged chemical concentration is different for each experiment.

From these experiments, we conclude that thermohaline convection is almost intrinsically chaotic at low porosity $\phi = 0.01$. We attribute this instability to a dominance of chemical transfer over the moderate heat transfer that actually drives the flow. Since advection and dispersion of chemicals dominate over molecular diffusion, the flow field appears unsteady.

The flow is characterized by the coexistence of advective and diffusive areas. Moreover, fast upward advective transport and lateral mixing of solute spontaneously leads to the generation of horizontal chemical interfaces at depth. Since the chemical difference across the interface results in a stable density interface, separately convecting and chemically distinct layers develop on top of each other. These layers either grow or decline by the processes of advective and dispersive entrainment across the density interface(s). The time scale involved with the formation and disappearance of these interfaces determines the period between the major fluctuations of the flow. This convective style is fundamentally different from flow at intermediate and high porosities, which often evolve towards the static diffusive state.

Since the transition to chaos in three-dimensional experiments of pure thermally driven convection occurs at a lower thermal Rayleigh number as compared to two-dimensional experiments [37], we expect that the observed intrinsic unsteadiness of low-porosity thermohaline convection is also present in a three-dimensional setting.

3.3. Anisotropic permeability and mechanical dispersion

Permeability is one of the most critical parameters governing the flow in geological systems. Unfortunately, it is also one of the most difficult parameters to measure in the field (due to problems of heterogeneity and scale). Still, the permeability field of both oceanic and continental crust is very likely anisotropic and heterogeneous [1–3,38–42].

Several linear stability studies address the onset of thermal and thermohaline convection in anisotropic media (e.g. [43]). Other studies have focused on the amount of heat transport at slightly supercritical Rayleigh numbers, e.g. [44]. Kvernold and Tyvand [45] reported results on steady state thermal convection in anisotropic media for anisotropy ratios ranging from 0.01 to 100 and for Rayleigh numbers up to approximately 10 times the critical Rayleigh number Ra_{cr} (where Ra_{cr} also varies with anisotropy). The influence of anisotropic permeability on the flow pattern for the oceanic crust was studied by Rosenberg et al. [39]. The reader is referred to Storesletten [46] for a review on convection in anisotropic media.

In this section, we are interested in the influence which anisotropic permeability has on the dynamics of low-porosity thermohaline convection. Therefore, we have performed a set of experiments in a medium with $\phi = 0.01$ in which the permeability ratios $K_r = K_x/K_z = 10$ and 0.1 have been considered. First, a thermal Rayleigh number of $Ra_T = 600$ is considered based on the vertical permeability, while the buoyancy ratio is varied between $R_p = 0$ and 3. The other parameters are similar to those previously presented.

Fig. 8a displays the flow space of the experiments in a medium with $K_r = 10$. For all buoyancy ratios, the flow appears unsteady. The most prominent difference between the observed dynamical behavior as compared with experiments in an isotropic medium is that the aspect ratios of the convection cells are larger. Here, the aspect ratio is defined as the width of a convection cell divided by its length. For low buoyancy ratios ($R_p \leq 0.25$), the flow pattern is characterized by a

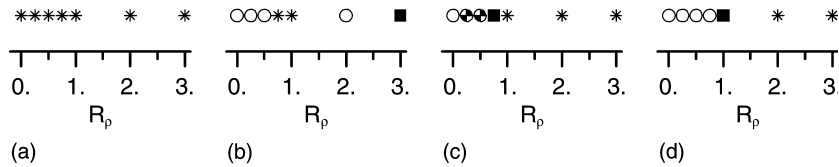


Fig. 8. Sensitivity of behavior of the flow to the anisotropic permeability of the rock, as a function of the buoyancy ratio R_p . Parameters are $Ra_T = 600$ and $\phi = 0.01$. The various flow states are explained in the caption of Fig. 7. (a) Permeability ratio is equal to $K_r = K_x/K_z = 10$. (b) $K_r = 0.1$. (c) Similar permeability ratio as in (a), $K_r = 10$, but now for an effective thermal Rayleigh number of $Ra_{T,eff} \approx 129.53$. (d) Similar permeability ratio as in (b), $K_r = 0.1$, but now for an effective thermal Rayleigh number of $Ra_{T,eff} \approx 1295.3$.

single convection cell. Oscillatory instabilities of the thermal boundary layers lead to a multi-periodic flow behavior. For larger buoyancy ratios, chemical interfaces develop again at depth and the flow appears very chaotic.

In Fig. 8b the flow space is shown as a function of R_p , for the case in which $K_r = 0.1$. For nearly all buoyancy ratios, the flow evolves to a steady state in which the aspect ratios of the cells are small, as compared to flow in isotropic media. The chaotic character of the flow at $R_p = 1$ is due to a nearly oscillatory bifurcation between a two-cellular flow pattern and that of a single slender convection cell and an adjacent diffusive area. The chemical reorganization involved with this bifurcation leads to an irregular behavior.

The differences between flow in isotropic and anisotropic media are primarily caused by the difference in the globally averaged permeability of these two media. In order to account for these linear effects of the anisotropy on the onset of convection and the vertical heat transport in thermally driven flow, Nield [47] proposed an effective thermal Rayleigh number $Ra_{T,eff}$ rather than a Rayleigh number based on the vertical permeability. This effective Rayleigh number is defined as:

$$Ra_{T,eff} = \frac{\alpha \rho g H \Delta T K_{SHR}}{\mu \kappa} \quad (11)$$

with:

$$K_{SHR} = 4 \left[\frac{1}{K_x^{1/2}} + \frac{1}{K_z^{1/2}} \right]^{-2}.$$

Using this $Ra_{T,eff}$, both the onset of convection and the heat transport efficiency do not depend

anymore on the degree of anisotropy. In order to investigate whether the transition from steady to chaotic thermochemical convection also scales with this effective $Ra_{T,eff}$, a set of experiments has been performed with the effective Rayleigh number as proposed by Nield [47].

Fig. 8c shows the case in which K_x is 10 times larger than K_z . In this case, $Ra_{T,eff} \approx 129.53$. For $R_p \leq 0.5$, the flow evolves either to a steady or an oscillatory convective state of two convection cells. The flow evolves through an initial chaotic stage towards the static diffusive solution when $R_p = 0.75$. For even larger buoyancy ratios, a single chaotic convection cell develops.

Fig. 8d shows the evolutionary states for various R_p , for a permeability ratio $K_r = 0.1$ ($Ra_{T,eff} \approx 1295.3$). For low buoyancy ratios, the flow evolves to a steady pattern consisting of 4–6 side-by-side convection cells. The flow evolves through an initial chaotic stage towards the static diffusive solution when $R_p = 1$. For $R_p \geq 2$, finally, the flow appears unsteady and it consists of slender convection cells together with diffusive areas. Furthermore, due to the development of chemical interfaces, intermittent stages of vertical layered convection are observed.

Comparison of the results of these experiments in anisotropic media with those obtained in isotropic ones (Fig. 8c) indicates that, despite the use of a similar effective thermal Rayleigh number, we do not obtain a similar transition to chaos as compared with isotropic media. Irrespective of the anisotropic character of the permeability, however, the flow appears chaotic for almost all buoyancy ratios.

Convective fluid flow through heterogeneous media is beyond the scope of this study. For

a detailed investigation of thermal convection through heterogeneous country rocks during contact metamorphism, the reader is referred to the simulations with stochastic permeability models of Gerdes et al. [14].

Mechanical dispersion of chemical concentration is another important factor which may influence the dynamics of the flow considerably. The amount of solute dispersion is related to the characteristic dispersion lengths of the porous medium: the longitudinal a_l and transversal a_t dispersivities. Like the degree of anisotropy in permeability, these two parameters also vary considerably among hydrothermal systems. Furthermore, they are not well-constrained from field measurements for km scale flow domains. Measured in situ values of longitudinal dispersivity are of the order of 1–50 m, while the transversal component is up to an order lower [48,49].

In the previous experiments, we have used the dimensionless dispersivities of $\hat{a}_l = 5 \times 10^{-4}$ and $\hat{a}_t = 5 \times 10^{-5}$, which correspond to the dimensional values of 2 and 0.2 m for a system of 4 km depth, respectively. Though these values are in the range of measured values, they can also easily be larger by more than an order of magnitude. In order to study the sensitivity of the flow dynamics to chemical dispersion explicitly, we have increased the dispersivities to $a_l = 40$ m and $a_t = 10$ m. The permeability is assumed to be isotropic again.

Fig. 9a, displays the evolution of the flow for $Ra_T = 600$ and $\phi = 0.01$, as a function of R_p . We find this evolution to closely resemble the case with lower dispersion lengths. This becomes evident from a comparison of Fig. 9a with the results for $Ra_T = 600$ in Fig. 7c. Nevertheless, some differences between the flow in the two media are observed. From the results, we have the following indications for the dynamical consequences of mechanical dispersion. Locally, larger dispersion lengths of the medium lead to a more uniform chemical concentration. On the scale of the whole domain, however, the global averaged fluctuations of chemical concentration are large, as compared with the simulations in media with low dispersivities. This can be seen in Fig. 9b in which the domain-averaged chemical concentration is plot-

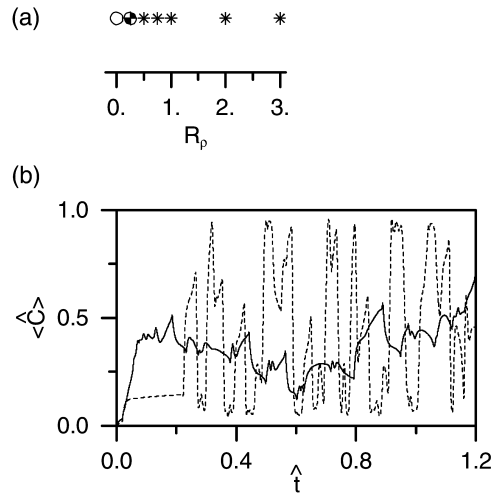


Fig. 9. (a) Various flow states for the case of larger dispersion lengths for chemical concentration ($\hat{a}_l = 1 \times 10^{-3}$ and $\hat{a}_t = 2.5 \times 10^{-4}$), as a function of the buoyancy ratio R_p . The other parameters are $Ra_T = 600$ and $\phi = 0.01$. The various flow states are explained in the caption of Fig. 8. (b) Domain-averaged chemical concentration plotted as a function of time for the high dispersion ($\hat{a}_l = 1 \times 10^{-3}$ and $\hat{a}_t = 2.5 \times 10^{-4}$, solid curve) and low dispersion model ($\hat{a}_l = 5 \times 10^{-4}$ and $\hat{a}_t = 5 \times 10^{-5}$, dotted). Parameters are $Ra_T = 600$, $R_p = 1$ and $\phi = 0.01$.

ted against time, for the two dispersivities. Parameters are $Ra_T = 600$, $R_p = 1$ and $\phi = 0.01$.

From these experiments in a low-porosity medium, we conclude that the convection dynamics depend significantly on the typical anisotropic and dispersive character of the rocks. While anisotropy changes the pattern of the flow in a characteristic manner, the transition from steady to chaotic behavior is different from the transition path followed in isotropic media. The characteristic dispersive length scales of the medium, on the other hand, do not change the typical dynamical behavior of the system, but do influence the interior C field evolution. Irrespective of the structural character of the rock, however, our results indicate that the dynamical behavior of thermohaline flow at low porosity ($\phi = 0.01$) is almost under all circumstances chaotic.

4. Discussion and conclusions

A large volume of the Earth's outer crust of

order $3 \times 10^9 \text{ km}^3$ is characterized by a porosity which is as small as one volume percent or less. However, fluids are commonly present and may remain so to depths of the order 5–15 km, as based on deep borehole measurements, oxygen isotope systematics of exhumed metamorphic terrains and analysis of obducted ophiolites and mesozonal granitic rocks. These deep fluids may convect through the rocks, driven by both thermal and chemical buoyancy; the former in response to the geothermal gradient and the latter due to differences in salinity that appear to be ubiquitous.

We have investigated the stability and dynamics of thermochemically driven convective flow in these low-porosity environments ($\phi=0.01$), as a function of thermal and chemical buoyancy. Despite the stabilizing gravitational influence of the solute, increasing the salinity contrast between top and bottom of the domain (while keeping the temperature contrast constant) leads to a transition from steady to chaotic behavior of the convection. For typical geological parameters, the onset of chaotic convection occurs when, at least for the two-dimensional flow studied here, the salinity contrast is approximately 5 wt% or more. Considering the large salinity gradients present within the crust, we conclude that advection of aqueous fluids appears intrinsically unsteady within vast volumes of the Earth's crust.

The chaotic dynamical behavior of the flow is due to the dominance of advective and dispersive chemical transfer over the more moderate convective heat transfer, the latter actually driving the flow. The flow pattern consists of distinct areas, in which heat and solute transport is governed either by advection or completely by diffusion. Furthermore, fast advective transport of solute enables the convective flow to spontaneously form horizontal chemical barriers at depth. These gravitationally stable interfaces divide the domain into two or more separately convecting layers of different composition. Advective and dispersive entrainment across the interfaces results in either upward or downward migration of the interfaces.

The convective style of low-porosity flow is fundamentally different from flow at intermediate porosity ($\phi=0.1$), which often evolves towards the

static diffusive state at larger buoyancy ratios. This instability is therefore restricted to crust with up to a few volume percents porosity.

The chaotic behavior of the flow evidently leads to an unsteadiness of the heat and solute transport across the domain. Within periods of only a few decades, the salinity content of the fluid can change from almost zero to almost the saturation level at one location. The periods between these fluctuations correspond with the time of the development and disappearance of the chemical interfaces. Further, increasing the solute contrast results in a significant decrease in the kinetic energy of the flow (not shown) and, related with this, the volume flux. Moreover, the heat flow is reduced considerably.

The convection dynamics depend significantly on the anisotropic character of permeability and on the specific dispersive character of the rocks. While anisotropy of permeability changes the pattern of the convective flow in a characteristic manner, the typical dispersive length scales of the medium mainly influence the chemical content of the fluid. Irrespective of the structural character of the rocks, however, our results indicate that the dynamical behavior of thermohaline flow at low porosity ($\phi=0.01$) appears intrinsically unsteady.

The unsteady flow has implications for various hydrogeological processes like heat transport through the crust, ore genesis, metasomatism, metamorphic petrology and the diagenetic history of sedimentary rocks in subsiding basins. Therefore, caution must be taken when assuming a steady convective flow field in the interpretation of fluid inclusion and stable isotope data in hydrothermally altered crustal rocks. The results presented here suggest that small differences in the spatial pattern of ϕ even lead to further instabilities. Finally, the intrinsic unsteadiness of chemically reactive flows [35,50] follows naturally from the hydrological unsteadiness shown.

Acknowledgements

Ron Trompert is thanked for his efforts during the development of the numerical method. The

investigations were supported by the Research Council for Earth and Lifesciences (ALW/NWO), within the project 750.195.08. Most of the computations were performed on the Cray Y-MP C916 at the Academic Computing Centre (SARA), Amsterdam, The Netherlands, within the project SC-492. Use of these computing facilities was sponsored by the National Computing Facilities Foundation (NCF). F.J.S. acknowledges support from NSF (EAR-9627800), DOE (DE-FG03-91ER-14211) and ICS 0337-49CM. [CL]

References

- [1] A.T. Fisher, Permeability within the basaltic oceanic crust, *Rev. Geophys.* 36 (1998) 143–192.
- [2] E. Huenges, J. Erzinger, J. Kück, B. Engeser, W. Kessels, The permeable crust: Geohydraulic properties down to 9101 m depth, *J. Geophys. Res.* 102 (1997) 18255.
- [3] C.E. Manning, S.E. Ingebritsen, Permeability of the continental crust: Implications of geothermal data and metamorphic systems, *Rev. Geophys.* 37 (1999) 127–150.
- [4] P. Mööller, S.M. Weise, E. Althaus, W. Bach, H.J. Behr, R. Borchardt, Paleofluids and recent fluids in the upper continental crust: Results from the German Continental Deep Drilling Program (KTB), *J. Geophys. Res.* 102 (1997) 18233–18254.
- [5] E. Lüschen, S. Sobolev, U. Werner, W. Söller, K. Fuchs, B. Gurevisch, P. Hubral, Fluid reservoir (?) beneath the KTB drillbit indicated by seismic shear-wave observations, *Geophys. Res. Lett.* 20 (1993) 923–926.
- [6] Y.A. Kozlovsky, The Superdeep Well of the Kola Peninsula, Springer-Verlag, New York, 1984.
- [7] P. Nehlig, Fracture and permeability analysis in magmahydrothermal transit ion zones in the Samail ophiolite (Oman), *J. Geophys. Res.* 99 (1994) 589–601.
- [8] B.E. Nesbitt, K. Muehlenbachs, Stable isotopic constraints on the nature of the syntectonic fluid regime of the Canadian Cordillera, *Geophys. Res. Lett.* 18 (1991) 963–966.
- [9] J.W. Valley, H.P. Taylor Jr. and J.R. O’Neil, *Rev. Mineral.* 16 (1986).
- [10] J.S. Hanor, Origin of saline fluids in sedimentary basins, in: J. Parnell (Ed.), *Geofluids: Origin of Fluids in Sedimentary Basins*, Geological Society of London special Publication 78, 1994, pp. 151–174.
- [11] M.J. Bickle, D. McKenzie, The transport of heat and matter by fluids during metamorphism, *Contrib. Mineral Petrol.* 95 (1987) 384–392.
- [12] L.M. Cathles, Scales and effects of fluid flow in the upper crust, *Science* 248 (1990) 323–329.
- [13] K.P. Furlong, R.B. Hanson and J.B. Bowers, Modeling thermal regimes, in: *Contact Metamorphism*, *Rev. Mineral.* 26, Mineral. Soc. of Am., Washington, DC, 1991, pp. 437–505.
- [14] M.L. Gerdes, L.P. Baumgartner, M. Person, Convective fluid flow through heterogeneous country rocks during contact metamorphism, *J. Geophys. Res.* 103 (1998) 23983–24003.
- [15] E. Tentorey, C.H. Scholz, E. Aharonov, A. Léger, Precipitation sealing and diagenesis 1. Experimental results, *J. Geophys. Res.* 103 (1998) 23951–23967.
- [16] E. Aharonov, E. Tentorey, C.H. Scholz, Precipitation sealing and diagenesis 2. Theoretical analysis, *J. Geophys. Res.* 103 (1998) 23969–23981.
- [17] M. Person, J.P. Raffensperger, S. Ge, G. Garven, Basin-scale hydrogeologic modeling, *Rev. Geophys.* 34 (1996) 61–87.
- [18] S.E. Ingebritsen and W.E. Sanford, *Groundwater in Geological Processes*, Cambridge University Press, Cambridge, 1998.
- [19] A.E. Scheidegger, General theory of dispersion in porous media, *J. Geophys. Res.* 66 (1961) 3273–3278.
- [20] D.A. Nield and A. Bejan, *Convection in Porous Media*, Springer-Verlag, New York, 1992.
- [21] M. Kaviany, *Principles of Heat Transfer in Porous Media*, Springer-Verlag, New York, 1991.
- [22] O.M. Phillips, *Flow and Reactions in Permeable Rocks*, Cambridge University Press, New York, 1991.
- [23] B.T. Murray, C.F. Chen, Double-diffusive convection in a porous medium, *J. Fluid Mech.* 201 (1989) 147–166.
- [24] H. Darcy, *Les Fontaines Publiques de la Ville de Dijon*, Victor Dalmont, Paris, 1856.
- [25] P.A. Tyvand, L. Storesletten, Onset of convection in an anisotropic porous medium with oblique principal axes, *J. Fluid Mech.* 226 (1991) 371–382.
- [26] J. Bear, *The Dynamics of Fluids in Porous Media*, Dover Publications, New York, 1972.
- [27] R.A. Trompert, U. Hansen, The application of a finite volume multigrid method to three dimensional flow problems in a highly viscous fluid with a variable viscosity, *Geophys. Astrophys. Fluid Dyn.* 83 (1996) 261–291.
- [28] W. Hundsdoerfer, R.A. Trompert, Method of lines and direct discretization: A comparison for linear advection, *Appl. Numer. Math.* 13 (1994) 469–490.
- [29] S. Kimura, G. Schubert, J.M. Straus, Route to chaos in porous-medium thermal convection, *J. Fluid Mech.* 166 (1986) 305–324.
- [30] N.D. Rosenberg, F.J. Spera, Thermohaline convection in a porous medium heated from below, *Int. J. Heat Mass Transfer* 35 (1992) 1261–1273.
- [31] C.M. Oldenburg, K. Pruess, Dispersive transport dynamics in a strongly coupled groundwater-brine flow system, *Water Resour. Res.* 31 (1995) 289–302.
- [32] S. Schoofs, R.A. Trompert, U. Hansen, The formation and evolution of layered structures in porous media, *J. Geophys. Res.* 103 (1998) 20843–20858.
- [33] S. Schoofs, R.A. Trompert and U. Hansen, The forma-

- tion and evolution of layered structures in porous media: Effects of porosity and mechanical dispersion, in revision for *Phys. Earth Planet. Int.* (1999).
- [34] E.W. Bolton, A.C. Lasaga, D.M. Rye, A model for the kinetic control of quartz dissolution and precipitation in porous media flow with spatially variable permeability: Formulation and examples of thermal convection, *J. Geophys. Res.* 101 (1996) 22157–22187.
- [35] E. Roedder, Fluid inclusions, *Rev. Mineral.* 12 (1984).
- [36] P.J. Saccocia, K.M. Gillis, Hydrothermal upflow zones in the oceanic crust, *Earth Planet. Sci. Lett.* 136 (1995) 1–16.
- [37] G. Schubert, J.M. Straus, Three-dimensional and multicellular steady and unsteady convection in fluid-saturated porous media at high Rayleigh numbers, *J. Fluid Mech.* 94 (1979) 25–38.
- [38] L.P. Baumgartner, M.L. Gerdes, M. Person and G.T. Roselle, Porosity and permeability of carbonate rocks during metamorphism, in: B. Jamtveit and B.M.D. Yardley (Eds.), *Fluid Flow and Transport in Rocks: Mechanisms and Effects*, Chapman and Hall, New York, 1997, pp. 83–98.
- [39] N.D. Rosenberg, F.J. Spera, R.M. Haymon, The relationship between flow and permeability field in seafloor hydrothermal systems, *Earth Planet. Sci. Lett.* 116 (1993) 135–153.
- [40] C. Clauser, Permeability of crystalline rocks, *EOS Trans.* 73/21, 233 (1992) pp. 237–238.
- [41] W.F. Brace, Permeability of and argillaceous crystalline rocks, *Int. J. Rock Mech. Min. Sci. Geomech. Abstr.* 17 (1980) 241–251.
- [42] W.F. Brace, Permeability of crystalline rocks: New in situ measurements, *J. Geophys. Res.* 89 (1984) 4327–4330.
- [43] G. Castinel, M. Combarrous, Natural convection in an anisotropic porous layer, *Int. Chem. Eng.* 17 (1976) 605–613.
- [44] R. McKibbin, Thermal convection in a porous layer effects of anisotropy and surface boundary conditions, *Transp. Porous Media* 1 (1986) 271–292.
- [45] O. Kvernfold, P.A. Tyvand, Nonlinear thermal convection in anisotropic porous media, *J. Fluid Mech.* 90 (1979) 609–624.
- [46] L. Storesletten, Effects of anisotropy on convective flow through porous media, in: D.B. Ingham and I. Pop (Eds.), *Transport Phenomena in Porous Media*, Pergamon Press, New York, 1998, pp. 261–283.
- [47] D.A. Nield, Notes on convection in a porous medium (i) an effective Rayleigh number for an anisotropic layer, (ii) the Malkus hypothesis and wavenumber selection, *Transp. Porous Media* 27 (1997) 135–142.
- [48] L.W. Gelhar, C. Welty, K.R. Rehfeldt, A critical review of data on field-scale dispersion in aquifers, *Water Resour. Res.* 28 (1992) 1955–1974.
- [49] D. Schulze-Makuch, D.S. Cherkauer, Method developed for extrapolating scale behavior, *EOS Trans.* 78 (1997) 3–4.
- [50] C.I. Steefel, A.C. Lasaga, A coupled model for transport of multiple chemical species and kinetic precipitation/dissolution reactions with application to reactive flow in single phase hydrothermal systems, *Am. J. Sci.* 294 (1994) 529–592.